

C2FUEL - This project has received funding from the European Union's Horizon 2020 research and innovation programme under grant agreement No 838014

The C2FUEL project results presented reflect only the author's view. The Commission is not responsible for any use that may be made of the information it contains.



Carbon Captured Fuel and Energy Carriers for an  
Intensified Steel Off-Gases based Electricity Generation in  
a Smarter Industrial Ecosystem

# Deliverable

D2.4– Influence of sweeping gases on the single cells  
performance and durability

WP2 – High temperature electrolysis development

## Project information

Grant Agreement n°	838014
Dates	1 <sup>st</sup> June 2019 – 30 <sup>th</sup> November 2023

### PROPRIETARY RIGHTS STATEMENT

This document contains information, which is proprietary to the C2FUEL Consortium. Neither this document nor the information contained herein shall be used, duplicated or communicated by any means to any third party, in whole or in parts, except with prior written consent of the C2FUEL consortium.

## Document Status

### Document information

<b>Deliverable name</b>	Influence of sweeping gases on the single cells performance and durability
<b>Responsible beneficiary</b>	XIUFU SUN / DTU
<b>Contributing beneficiaries</b>	MATTI NOPONEN / ELCOGEN
<b>Contractual delivery date</b>	M35 – 30/04/2022
<b>Actual delivery date</b>	M37 – 02/06/2022
<b>Dissemination level</b>	Public

### Document approval

Name	Position in project	Organisation	Date	Visa
P. OLIVIER	Coordinator	ENGIE	25/05/2022	OK
L. NAIGLIN	Project Management Officer	BENKEI	25/05/2022	OK
A. MIQUELOT	Project Management Officer	ENGIE	25/05/2022	OK
M.NOPONEN	WP2 LEADER	ELCOGEN	02/06/2022	OK

### Document history

Version	Date	Modifications	Authors
V1	28/02/2022	1 <sup>ST</sup> DRAFT	X. Sun / DTU
V2	16/05/2022	Second version	X. Sun / DTU , A. Miquelot / ENGIE
V3	20/05/2022	Third version	Xiufu Sun / DTU
VF	02/06/2022	Quality check / Final version	L. Naiglin / BENKEI, A. Miquelot BENKEI / M. Noponen ELCOGEN

## Table of Contents

<b>Document Status</b> .....	<b>1</b>
<b>List of Figures</b> .....	<b>3</b>
<b>Deliverable report</b> .....	<b>4</b>
<b>1 Executive Summary</b> .....	<b>4</b>
1.1 Description of the deliverable content and purpose	
1.2 Brief description of the state of the art and the innovation breakthroughs	
1.3 Corrective action (if relevant)	
1.4 IPR issues (if relevant)	
<b>2 Introduction</b> .....	<b>5</b>
<b>3 Experimental</b> .....	<b>5</b>
<b>4 Results and discussion</b> .....	<b>6</b>
4.1 Initial performance characterization	
4.2 Durability under current	
4.3 EIS analysis during durability test	
<b>5 Post-test analysis</b> .....	<b>11</b>
<b>6 Conclusion</b> .....	<b>12</b>
<b>7 References</b> .....	<b>13</b>

## List of Figures

Figure 1: iV characterization under 700 °C with 50%H <sub>2</sub> + 50%H <sub>2</sub> O supplied to the fuel electrode and Air supplied to the oxygen electrode of the four tested cells. ....	6
Figure 2: Cell voltage evolution during the durability tests of the three tested cells. Current density was -0.5 A/cm <sup>2</sup> throughout the period in all three tests. ....	7
Figure 3: Serial resistance, polarization resistance and ASR extracted from the EIS measured during the durability test.....	8
Figure 4: Fuel electrode (a) and oxygen electrode (b) gas shift EIS and DRT analysis. ....	9
Figure 5: EIS and DRT analysis of the impedance measured during the durability test.....	10
Figure 6: XRD analysis on the oxygen electrode surface of the tested cells. ....	11
Figure 7: SEM analysis of the oxygen electrode surface of the four tested cells.....	12

## Deliverable report

### 1 Executive Summary

#### 1.1 Description of the deliverable content and purpose

In this deliverable, the influence of oxygen electrode sweep gas on solid oxide single cells performance and durability will be reported.

#### 1.2 Brief description of the state of the art and the innovation breakthroughs

Studies on durability of SOEC are mostly focused on the fuel electrode. Very limited studies exist on the influence of oxygen electrode sweep gas on the SOEC durability. The results from this study showed that no extra degradation was observed on the cell without sweep gas, while higher degradation was seen on the cell with CO<sub>2</sub> as oxygen electrode sweep gas.

#### 1.3 Corrective action (if relevant)

The description of action of the project specifies that “single cell tests will be performed [DTU] with different sweeping gas to the oxygen electrode air, H<sub>2</sub>O or CO<sub>2</sub> or even operating without sweeping gas.” However, additional studies from [DTU] revealed that H<sub>2</sub>O has a detrimental effect on the cell by severely damaging it (results will be presented at the European Fuel cell Forum (EFCE) 2022). Moreover, considering the balance of plant design and the energy loss associated to H<sub>2</sub>O evaporation at inlet and condensation at the outlet, the use of H<sub>2</sub>O as purge gas does not appear anymore as a viable solution. Therefore, it was decided not to test H<sub>2</sub>O as sweeping gas for the oxygen electrode and efforts have been devoted to study whether increasing H<sub>2</sub> concentration at the fuel electrode could lead to lower cell degradation rate.

#### 1.4 IPR issues (if relevant)

Non applicable.

## 2 Introduction

Long term durability of many thousands hours of operation with such SoA cells have been demonstrated both on single cell and stack level[1–7]. While most of the studies were focused on the hydrogen or syngas production from SOECs, only a few works have addressed the utilization of the produced oxygen[8–10]. Oxygen is an important industrial gas that is widely used in industrial/chemical processes as well as medical and life-support systems. Oxygen nowadays is mostly produced at large scale via cryogenic air separation units (ASU) and via pressure swing adsorption (PSA) methods for small units. SOEC in theory can produce 100% purity of oxygen and has the advantage of scale flexibility compared with the ASU. Most studies on SOEC stack operation were performed with air supplied to the oxygen electrode compartment mostly due to the safety concerns and stack heat management, while on the single cell level both air and oxygen purge has been widely used. By using oxygen as purge gas, it is possible to avoid the voltage transition due to the change of oxygen partial pressure on the oxygen electrode upon changing the electrolysis current, this facilitates data interpretation when the aim is detailed performance characterization. In principle SOEC can be operated without any purge gas as it produces O<sub>2</sub> during electrolysis operation. Purging with another gas such as CO<sub>2</sub> could be interesting for two reasons; 1) it reduces the O<sub>2</sub> concentration in the oxygen electrode exhaust gas improving safety, and 2) it provides a hot oxygen enriched gas that can be directly utilized in oxy-combustion processes to replace air (eliminating N<sub>2</sub> dilution). The effect of different purge gases on the degradation of SOECs however is not well studied. In this work, we report on a durability study of SOECs operated for steam electrolysis with air, no gas and CO<sub>2</sub> supplied to the oxygen electrode in three otherwise identical SOEC single cell test. Detailed electrochemical analysis was performed to analyze the origin of observed degradation.

## 3 Experimental

Three SOECs from the same production batch made by [ELCOGEN] were used in this study, one of them served as the reference cell where only initial performance characterizations were carried out, the other three were used for durability test. The cells to be used for the specific test runs are in the following denoted: *Cell\_air*, *Cell\_nan*, *Cell\_co2* for cells tested with air, no gas and CO<sub>2</sub> purge gas to the oxygen electrode, respectively. The cells consists of a ~400 μm Ni/YSZ (yttria stabilized zirconia) support layer having a ~12 μm Ni/YSZ active layer, a ~3μm YSZ electrolyte and a CGO (gadolinium-doped ceria) barrier layer of similar thickness and a ~12 μm thick LSC (lanthanum strontium cobaltite) oxygen electrode[11]. For testing, the cell was mounted in an alumina cell test house[12]. Ni plates and Ni meshes were used as fuel electrode current collector and gas distribution component, Au plates and Au meshes were used as oxygen electrode current collector and gas distribution components. An Au frame was used for sealing the fuel electrode compartment and no sealing was applied for the oxygen electrode side. The cells were heated to 850 °C with a ramp rate of 1 °C/min, 20 L/h N<sub>2</sub> was supplied to the fuel electrode compartment and 20 L/h air was supplied to the oxygen electrode during heating. The NiO in the cell was reduced in 20 L/h of 5% H<sub>2</sub> + N<sub>2</sub> for 2 hours then H<sub>2</sub> + 4% H<sub>2</sub>O for 1 hour. The cell temperature was then brought to 800 °C for initial performance characterization. The initial performance characterization was performed from 800 to 650 °C with 50 °C /step in 24 L/h H<sub>2</sub> with 4, 20, 50, 90% H<sub>2</sub>O supplied to the fuel electrode and a 140 L/h of air

flow supplied to the oxygen electrode. Current-voltage curves (iV) and electrochemical impedance spectra (EIS) characterization were carried out at each characterization point. EIS were measured at zero current (open circuit voltage) using a Solartron 1255B frequency analyzer and an external shunt connected in series with the cell. The spectra were recorded from 96850 to 0.08 Hz with 12 points per decade and were corrected using the short circuit impedance response of the test setup. From the impedance spectra, the ohmic (serial) area specific resistance ( $R_s$ ) was taken as the value of the real part of the impedance measured at 96850 Hz and the polarization area specific resistance ( $R_p$ ) was taken as the difference in the real part of the impedance at 96850 Hz and 0.08 Hz. The total area specific resistance of a cell was calculated as the sum of the real part of the impedance ( $R_s + R_p$ ).

The durability tests were performed at 700 °C at  $-0.5 \text{ A/cm}^2$  with 6.7 L/h of 10%  $\text{H}_2 + 90\% \text{H}_2\text{O}$  supplied to the fuel electrode. The gas supplied to the oxygen electrode was 140 L/h Air for *Cell\_air*, 10 L/h  $\text{CO}_2$  for *Cell\_co2* and no gas was supplied to the oxygen electrode for the *Cell\_nan* test. The theoretical  $\text{H}_2\text{O}$  conversion calculated based on Faraday's law is 58% and the corresponding oxygen partial pressure at the oxygen electrode is 22%, 14% and 100% for the *Cell\_air*, *Cell\_co2* and *Cell\_nan*. EIS characterizations were performed under current during the durability test.

## 4 Results and discussion

### 4.1 Initial performance characterization

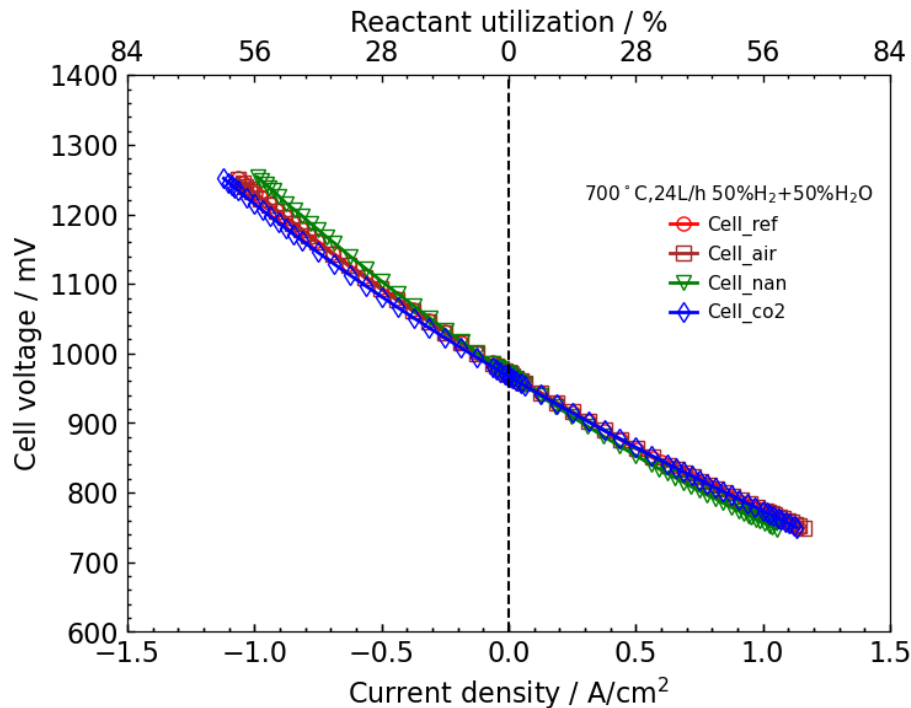


Figure 1: iV characterization under 700 °C with 50% $\text{H}_2 + 50\% \text{H}_2\text{O}$  supplied to the fuel electrode and Air supplied to the oxygen electrode of the four tested cells.

Figure 1 presents the initial iV characterization of the four tested cells at 700 °C with 50% $H_2$  + 50% $H_2O$  supplied to the fuel electrode compartment and air supplied to the oxygen electrode compartment. The open circuit voltages are 972, 971, 970 and 968 mV for *Cell\_ref*, *Cell\_air*, *Cell\_nan* and *Cell\_co2* respectively, which are very close to the theoretical value of 973mV calculated by Nernst equation based on the temperature and gas composition, indicating the good sealing and gas tightness of the electrolyte. The cells exhibit very good reproducibility in performance, only minor differences can be seen where *Cell\_nan* shows slightly low initial electrochemical performance than the others which may be due to minor differences in the cell production or imperfect contacting during cell mounting.

## 4.2 Durability under current

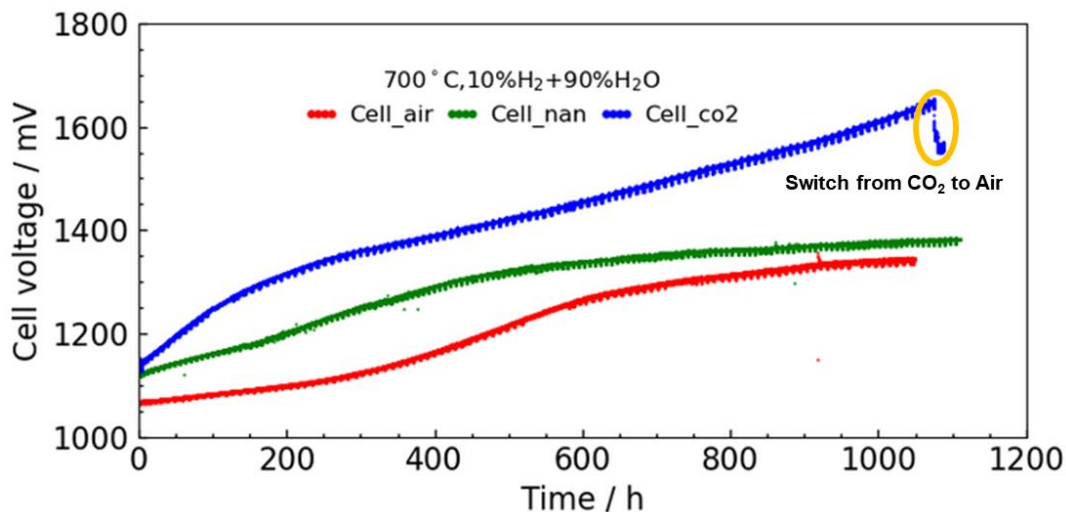


Figure 2: Cell voltage evolution during the durability tests of the three tested cells. Current density was  $-0.5 \text{ A/cm}^2$  throughout the period in all three tests.

Cell voltages were recorded during the constant current operation at 700 °C with 10%  $H_2$  + 90%  $H_2O$  supplied to the fuel electrode and air,  $CO_2$  or no purge gas at the oxygen electrode. The cell voltage evolution with operation time is presented in Figure 2. Different initial cell voltages under the same current load were observed between the three tested cells, *Cell\_air* started at 1067 mV, *Cell\_nan* started at 1118 mV and *Cell\_co2* started at 1133 mV. The higher initial voltage of *Cell\_nan* compared with *Cell\_air* may be due to both the slight difference in the initial performance (see Figure 1) as well as the difference in oxygen partial pressure at the oxygen electrode, where a theoretical increase of OCV of 33mV can be expected when changing the oxygen electrode compartment purge gas from air (883 mV) to oxygen (916 mV). The theoretical OCV for *Cell\_co2* when using  $CO_2$  to the oxygen electrode is expected to be lower than that of *Cell\_air* due to the lower oxygen partial pressure at the oxygen electrode for *Cell\_co2* (14%) than *Cell\_air* (22%). However, on *Cell\_co2* an increase of 13 mV when changing from no gas to  $CO_2$  supplied to the oxygen electrode compartment is observed (at the start of the test, close to 0h

as shown in Figure 2), which clearly indicated that the high initial voltage is an effect of the CO<sub>2</sub> purge. This can also be seen at the end of the durability test *Cell\_co2* as marked in orange circle area in Figure 2; by changing from CO<sub>2</sub> to no gas, and then to air supplied to the oxygen electrode, the cell voltage decreased from 1640 mV (CO<sub>2</sub>) to 1587 mV (no gas) then to 1557 mV (Air). Hence, there seems to be two effects of the purge with CO<sub>2</sub>: 1) an immediate resistance increase, as observed initially (increased voltage at the beginning of the durability test) and when doing the gas variation after the durability test, and 2) an increased degradation over the durability test period. The overall degradation for the three tested cells during the entire testing period, as measured in the form of a voltage increase are 264, 238, 464 mV/1000h for *Cell\_air*, *Cell\_nan* and *Cell\_co2* respectively. “Fast” initial degradation can be observed on all the three tested cells, the degradation rates for *Cell\_air* and *Cell\_nan* decreased after the initial period to 114 and 68 mV/1000h in the last 200 hours, respectively. The slightly lower degradation rates of *Cell\_nan* to *Cell\_air* in the last 200 hours might be related the impurities in the air stream, that caused oxygen electrode surface segregation [13] and thus higher degradation on *Cell\_air*. A clearly accelerated degradation, with a degradation rate of 443 mV/1000h, is observed on the test with CO<sub>2</sub> purge.

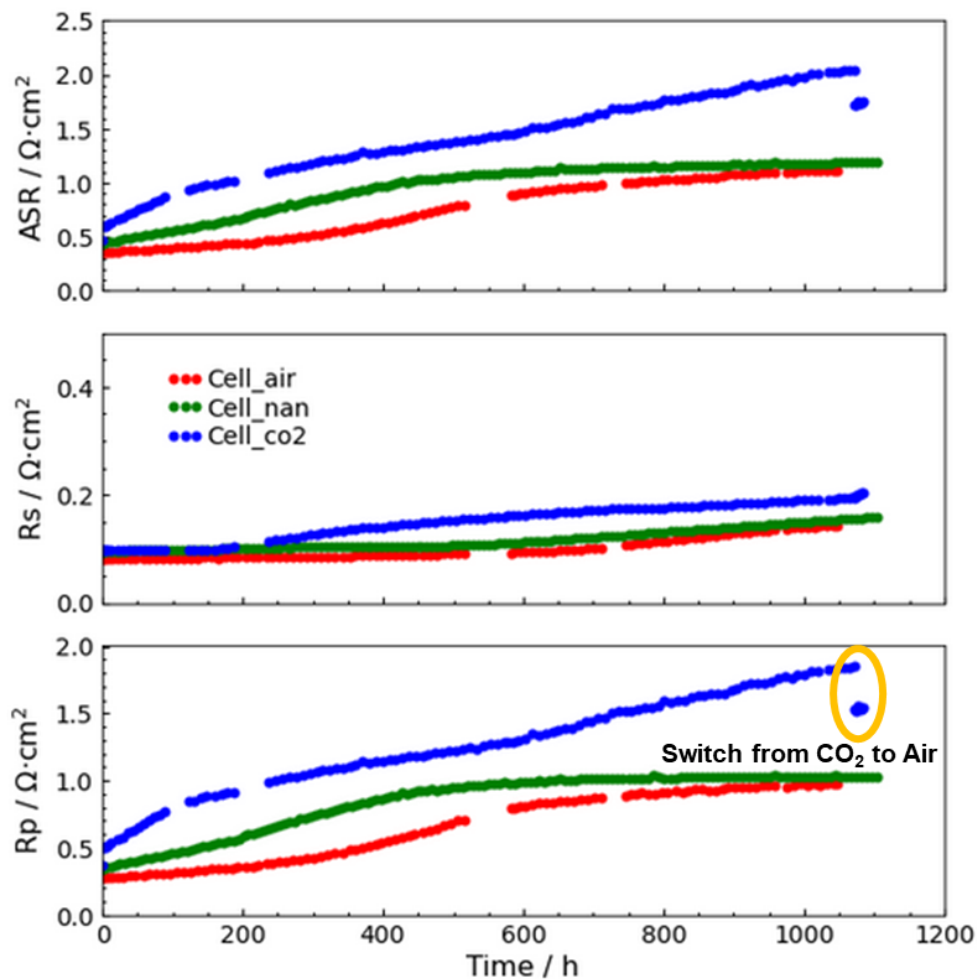


Figure 3: Serial resistance, polarization resistance and ASR extracted from the EIS measured during the durability test.

The serial area specific resistance ( $R_s$ ), polarization area specific resistance ( $R_p$ ) and area specific resistance (ASR) extracted from the EIS measured during the durability study are presented in Figure 3. At the beginning, the three cells show  $R_s$  values that are very close. A larger difference is, as expected, observed for the polarization resistance. *Cell\_air* and *Cell\_nan* exhibit a very similar  $R_s$ ,  $R_p$  and ASR degradation trend, with low  $R_s$  degradation rate and high  $R_p$  degradation rate in the first 500 hours but afterwards a high  $R_s$  degradation and low  $R_p$  degradation rate afterward. On the other hand, the *Cell\_co2* shows similar  $R_s$  evolution trend as the other two cells, but exhibits an accelerated  $R_p$  increase after the initial degradation. At the end of the durability test of *Cell\_co2*, a noticeable decrease in polarization resistance is seen on the *Cell\_co2*, when switching from CO<sub>2</sub> purge to air purge, indicating that the higher initial cell voltage and polarization seen from both Figure 2 and Figure 3 are mainly due to an increase of the polarization resistance. Such phenomena has also been reported on LSC materials used as cathodes in fuel cell mode[14,15]. The initial fast increase of polarization could be due to the microstructure changes in the fuel electrode, such as impurities precipitation/segregation [16], Ni coarsening and Ni migration away from the active electrode as a consequence of a deterioration of the Ni-Ni network. Such phenomena also results in an increase of  $R_s$  afterwards[17].

### 4.3 EIS analysis during durability test

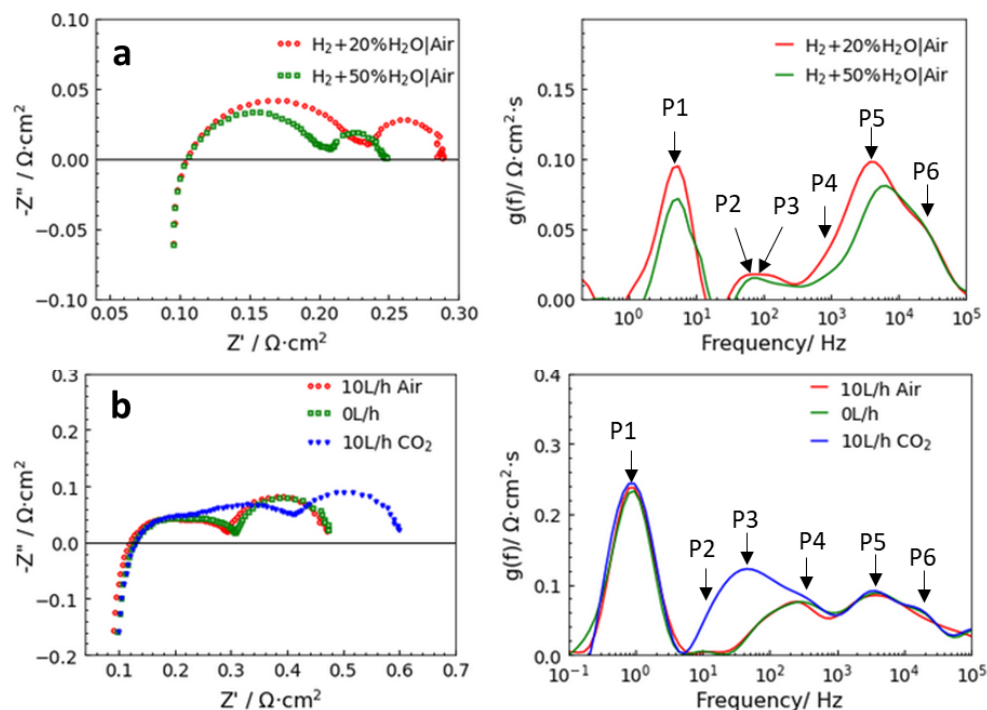


Figure 4: Fuel electrode (a) and oxygen electrode (b) gas shift EIS and DRT analysis.

Prior to durability test, gas shift impedance spectra were recorded for distribution of relaxation time (DRT) analysis in order to help identifying the different electrochemical processes and correlating them to the

corresponding electrodes. Gas shift EIS were performed at 700 °C. For fuel electrode, EIS were recorded at OCV with gas composition of 80% $H_2$  + 20% $H_2O$  and 20% $H_2$  + 80% $H_2O$  supplied to the fuel electrode while keeping constant air flow supplied to the oxygen electrode. The oxygen electrode gas shift EIS were performed under - 0.5 A/cm<sup>2</sup> by changing the oxygen electrode gas from 10 L/h air to no gas, and then to 10L/h  $CO_2$  while keeping constant 10%  $H_2$  + 90 %  $H_2O$  supplied to the fuel electrode. Figure 4 a and b present the Nyquist representation of recorded impedance spectra and corresponding DRT analysis results of fuel electrode and oxygen electrode gas shift. Six distinguishable peaks can be identified from the DRT figures. Upon changing the  $H_2O$  partial pressure, four noticeable process responses can be identified. Peak P4 and P5 with summit frequency at ca. 500-800 Hz and ca. 50 kHz, corresponding to the fuel electrode charge transfer reaction processes response with an increase of DRT peak. Also, the peak, P2, at ca. 80 Hz, corresponding to the gas diffusion process, and the peak P1 with summit frequency at ca. 3 Hz, attributed to the gas conversion process responds changes on the change of the “fuel” gas. The process P6 at ca. 20 kHz which does not change with  $H_2O$  partial pressure can likely be attributed to the ion transportation through the composite fuel electrode. The oxygen electrode peak P3, cannot be directly distinguished from the fuel electrode response due to overlapping with the gas diffusion process, but it can be clearly identified when changing the gas on the oxygen electrode to  $CO_2$  as evident in Figure 4b, where the DRT peak increases strongly at 50Hz upon introducing  $CO_2$ . No noticeable peak change can be seen when changing of sweep gas from air to no gas, however, a large peak increase of P3 can be seen at frequency range of 10-200 Hz upon changing to  $CO_2$  purge at the oxygen electrode. Hence, the  $CO_2$  surely impedes this process – which has in literature been ascribed to a reaction of  $CO_2$  and LSC oxygen electrode[15].

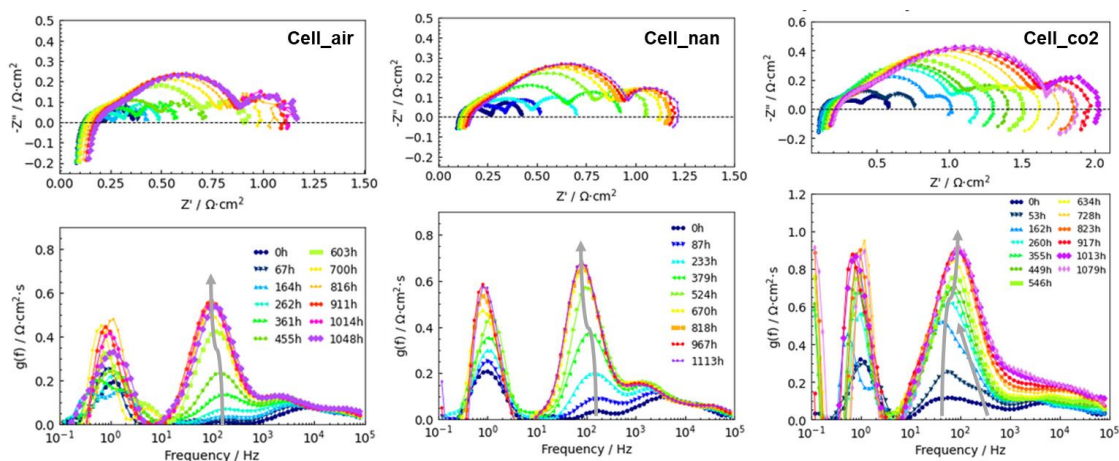


Figure 5: EIS and DRT analysis of the impedance measured during the durability test

Figure 5 presents the EIS measured during the durability test of the three cells. DRT analysis was applied to better represent frequency resolution of the recorded impedance data during the degradation process. It can be seen from the Nyquist plot in Figure 5 top figures that for all the three tests, both ohmic and polarization resistance increased during the durability test. At least four distinguishable peaks can be identified from the DRT plots. *Cell\_air* and *Cell\_nan* have a very similar degradation behavior in terms of peak evolution and corresponding changes in summit frequencies. Large peak increase and frequency shift can be seen for P4 and P5 at the frequency

range of 100-1kHz and 1-10 kHz for all the three tests as marked with gray arrow in the figures, both processes originating from the fuel electrode. An extra peak of P3 can be seen from the *Cell\_Co2*, where a significant increase of the peak at ca. 40 Hz can be identified, which overlapped with the process P4 at frequency of 100-1k Hz after 200h test. Such a process, however, is not seen on the *Cell\_air* and *Cell\_nan*. It is therefore clear that CO<sub>2</sub> has very negative effect on the cell durability. It is also clear, that at cell level it makes no difference on performance and durability whether to purge away the oxygen produced with air or age the cell in the atmosphere defined by the produced oxygen.

## 5 Post-test analysis

It is speculated that carbonate such as SrCO<sub>3</sub> formation might be the cause for the degradation/passivation of oxygen electrode, and literature has shown that CO<sub>2</sub> has a strong side effect on the LSC or LSCF based oxygen electrodes[14,15,18]. To detect any carbonate formation, X-ray diffraction (XRD) analysis was performed on the oxygen electrode surface of the tested samples and the results is presented in Figure 6.

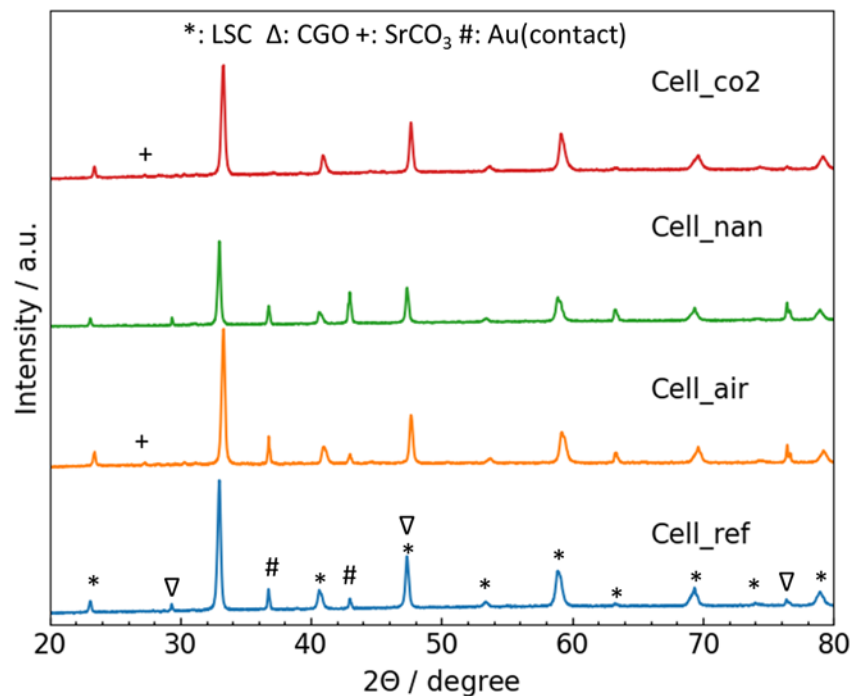


Figure 6: XRD analysis on the oxygen electrode surface of the tested cells.

Almost no detectable SrCO<sub>3</sub> formation is seen on the oxygen electrode surface of the tested cells, very small peaks may likely be related to SrCO<sub>3</sub>, which however appeared on both *Cell\_co2* and *cell\_air*, indicating that such a peak is not directly related to the CO<sub>2</sub> purge gas.

SEM analyses were carried out on the polished surface of the tested cells and focus was put on the oxygen electrode surfaces. Figure 7 presents the SEM results of the tested cells. The oxygen electrode of the tested cells showed very similar morphology compared with the reference cells, no noticeable difference was observed. It is therefore speculated that the influence of CO<sub>2</sub> on the oxygen electrode was mainly due to the surface adsorption

which blocked the active reaction site for oxygen evolution. The absorbed CO<sub>2</sub> was then swapped to O<sub>2</sub> and Air when CO<sub>2</sub> purge gas was stopped and switched to Air. The difference in the cell degradation is due to the uneven current distribution caused by CO<sub>2</sub> passivation of the oxygen electrode.

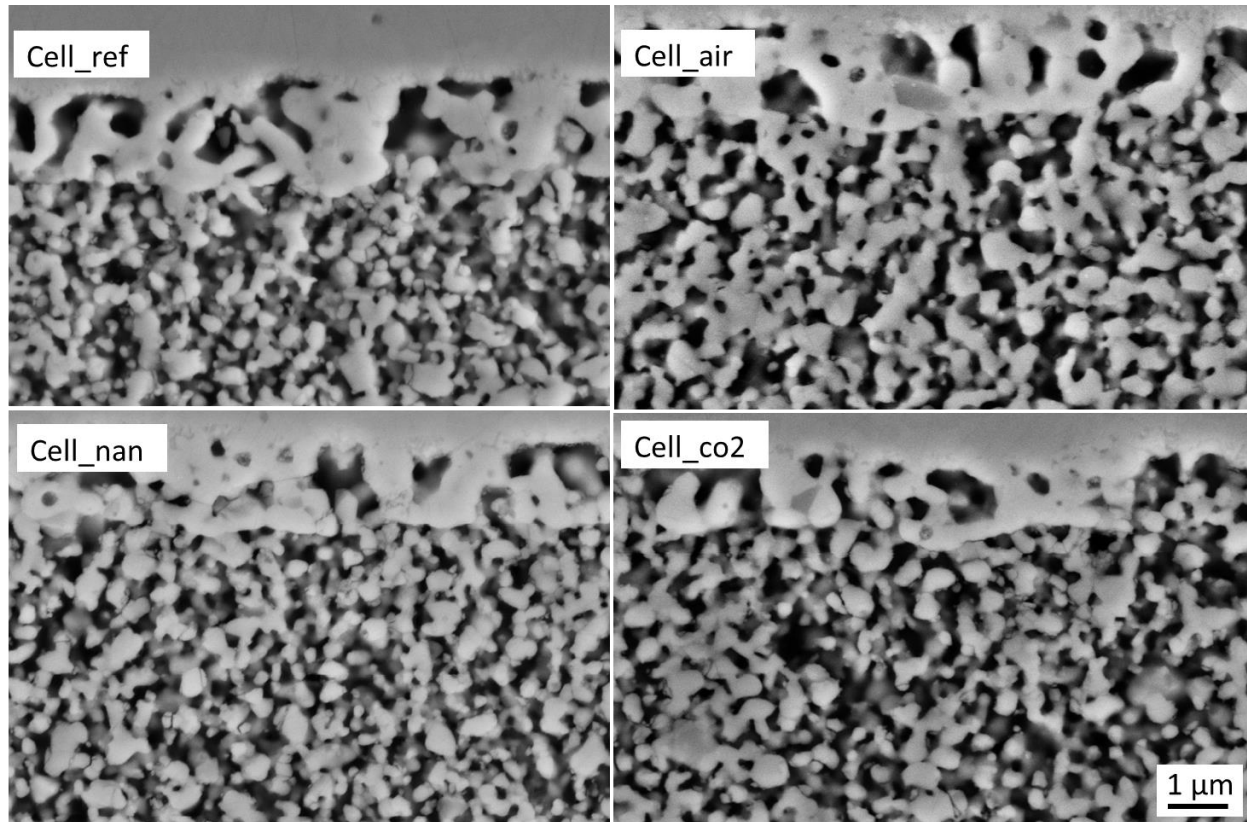


Figure 7: SEM analysis of the oxygen electrode surface of the four tested cells.

## 6 Conclusion

The effect of purge gas on the oxygen electrode on the durability of three SOECs under steam electrolysis condition have been studied. Purging SOEC with air or dosing no purge to the oxygen electrode compartment leads to similar overall degradation behavior. Slightly lower degradation rates in the last 200 h for the test, *Cell\_nan* with no purge, compared with *Cell\_air* could be due to air impurities. More tests would be however, needed to conclude on effects of impurities in the air stream. Using CO<sub>2</sub> as purge gas leads to higher degradation rates than air or no purge gas. There is both an immediate increase in electrode resistance when using CO<sub>2</sub> (which is partially removed when terminating the purge), and an increase in the Rp degradation rate. XRD analyses showed no difference in the SrCO<sub>3</sub> phase formation between Air and CO<sub>2</sub> as purge gases and SEM revealed the similar morphology of the oxygen electrode. Therefore, it is speculated that the influence of CO<sub>2</sub> on the oxygen electrode was mainly due to the surface absorption which blocked the active reaction site for oxygen evolution.

## 7 References

- [1] J. Schefold, A. Brisse, H. Poepke, 23,000 h steam electrolysis with an electrolyte supported solid oxide cell, *International Journal of Hydrogen Energy*. 42 (2017) 13415–13426. <https://doi.org/10.1016/j.ijhydene.2017.01.072>.
- [2] J. Schefold, A. Brisse, A. Surrey, C. Walter, 80,000 current on/off cycles in a one year long steam electrolysis test with a solid oxide cell, *International Journal of Hydrogen Energy*. 45 (2020) 5143–5154. <https://doi.org/10.1016/j.ijhydene.2019.05.124>.
- [3] G. Corre, A. Brisse, 9000 Hours Operation of a 25 Solid Oxide Cells Stack in Steam Electrolysis Mode, *ECS Transactions*. 68 (2015) 3481–3490. <https://doi.org/10.1149/06801.3481ecst>.
- [4] V.N. Nguyen, Q. Fang, U. Packbier, L. Blum, Long-term tests of a Jülich planar short stack with reversible solid oxide cells in both fuel cell and electrolysis modes, *International Journal of Hydrogen Energy*. 38 (2013) 4281–4290. <https://doi.org/10.1016/j.ijhydene.2013.01.192>.
- [5] J. Schefold, H. Poepke, A. Brisse, Solid Oxide Electrolyser Cell Testing Up to the Above 30,000 h Time Range, *ECS Trans*. 97 (2020) 553. <https://doi.org/10.1149/09707.0553ecst>.
- [6] Q. Fang, L. Blum, N.H. Menzler, D. Stolten, Solid Oxide Electrolyzer Stack with 20,000 h of Operation, *ECS Trans*. 78 (2017) 2885–2893. <https://doi.org/10.1149/07801.2885ecst>.
- [7] G. Rinaldi, S. Diethelm, E. Oveisi, P. Burdet, J.V. Herle, D. Montinaro, Q. Fu, A. Brisse, Post-test Analysis on a Solid Oxide Cell Stack Operated for 10,700 Hours in Steam Electrolysis Mode, *Fuel Cells*. 17 (2017) 541–549. <https://doi.org/10.1002/fuce.201600194>.
- [8] P. Iora, P. Chiesa, High efficiency process for the production of pure oxygen based on solid oxide fuel cell–solid oxide electrolyzer technology, *Journal of Power Sources*. 190 (2009) 408–416. <https://doi.org/10.1016/j.jpowsour.2009.01.045>.
- [9] J. Hartvigsen, S. Elangovan, J. Elwell, D. Larsen, Oxygen Production from Mars Atmosphere Carbon Dioxide Using Solid Oxide Electrolysis, *ECS Trans*. 78 (2017) 2953–2963. <https://doi.org/10.1149/07801.2953ecst>.
- [10] K.R. Sridhar, B.T. Vaniman, Oxygen production on Mars using solid oxide electrolysis, *Solid State Ionics*. 93 (1997) 321–328.
- [11] Solid Oxide Fuel Cells | Products, Elcogen. (n.d.). <https://elcogen.com/products/solid-oxide-fuel-cells/> (accessed May 27, 2021).
- [12] A. Hagen, X. Sun, B.R. Sudireddy, Å.H. Persson, Metal Supported SOFCs for Mobile Applications using Hydrocarbon Fuels, *J. Electrochem. Soc*. 167 (2020) 104510. <https://doi.org/10.1149/1945-7111/ab9b9d>.
- [13] K. Chen, S.P. Jiang, Surface Segregation in Solid Oxide Cell Oxygen Electrodes: Phenomena, Mitigation Strategies and Electrochemical Properties, *Electrochem. Energ. Rev.* 3 (2020) 730–765. <https://doi.org/10.1007/s41918-020-00078-z>.
- [14] Z. Zhao, L. Liu, X. Zhang, W. Wu, B. Tu, D. Ou, M. Cheng, A comparison on effects of CO<sub>2</sub> on La<sub>0.8</sub>Sr<sub>0.2</sub>MnO<sub>3+δ</sub> and La<sub>0.6</sub>Sr<sub>0.4</sub>CoO<sub>3-δ</sub> cathodes, *Journal of Power Sources*. 222 (2013) 542–553. <https://doi.org/10.1016/j.jpowsour.2012.09.023>.
- [15] J. Hayd, E. Ivers-Tiffée, Detailed Electrochemical Study on Nanoscaled La<sub>0.6</sub>Sr<sub>0.4</sub>CoO<sub>3-δ</sub> SOFC Thin-Film Cathodes in Dry, Humid and CO<sub>2</sub>-Containing Atmospheres, *J. Electrochem. Soc*. 160 (2013) F1197. <https://doi.org/10.1149/2.026311jes>.
- [16] A. Hauch, S.D. Ebbesen, S.H. Jensen, M. Mogensen, Solid Oxide Electrolysis Cells: Microstructure and Degradation of the Ni/Yttria-Stabilized Zirconia Electrode, *Journal of The Electrochemical Society*. 155 (2008) B1184. <https://doi.org/10.1149/1.2967331>.
- [17] X. Sun, P.V. Hendriksen, M.B. Mogensen, M. Chen, Degradation in Solid Oxide Electrolysis Cells During Long Term Testing, *Fuel Cells*. 19 (2019) 740–747. <https://doi.org/10.1002/fuce.201900081>.
- [18] Z. Zhao, L. Liu, X. Zhang, W. Wu, B. Tu, D. Cui, D. Ou, M. Cheng, High- and low- temperature behaviors of La<sub>0.6</sub>Sr<sub>0.4</sub>Co<sub>0.2</sub>Fe<sub>0.8</sub>O<sub>3-δ</sub> cathode operating under CO<sub>2</sub>/H<sub>2</sub>O-containing atmosphere, *International Journal of Hydrogen Energy*. 38 (2013) 15361–15370. <https://doi.org/10.1016/j.ijhydene.2013.09.089>.